International Journal of Thermophysics, Vol. 23, No. 3, May 2002 (© 2002)

Convective Effects During Diffusivity Measurements in Liquids with an Applied Magnetic Field

Y. Y. Khine,[1] R. M. Banish,[1,2] and J. I. D. Alexander[3]

Received September 19, 2001

Convective contamination of self-diffusion experiments with an applied magnetic field is considered using a two-dimensional axisymmetric model. Constant, uniform, and an additional non-uniform heat fluxes are imposed along the sidewall of the cylinder while constant heat loss occurs through the top and bottom. In this model, due to a very small thermal Péclet number, convective heat transfer is neglected, and the flow is steady and inertialess. Time-dependent concentration is solved for various values of the mass Péclet number, Pe_m, (the ratio between the convective transport rate and the diffusive transport rate) and different magnetic field strengths represented by the Hartmann number Ha. Diffusivities are obtained using the same algorithm used to extract diffusivity values from the actual experimental data. Normalized values of these diffusivities vs. effective Pe_m are presented for different imposed temperature profiles. In all cases, the diffusivity value obtained through the simulated measurement increases as the effective Pe_m increases. The numerical results suggest that an additional periodic flux, or "hot" and "cold" spots, can significantly decrease the convective contamination in our geometry. The number of periodicity in temperature does not have a significant impact on the diffusivity results. Keeping the top wall slightly warmer than the bottom wall has no effect on the diffusivities for this model.

KEY WORDS: convective contamination; liquid metals; magnetic field; mass diffusion.

[1] Center for Microgravity and Materials Research, VBRH E-39, University of Alabama in Huntsville, Huntsville, Alabama 35899, U.S.A.

[2] To whom correspondence should be addressed. E-mail: banishm@email.uah.edu

[3] Department of Mechanical and Aerospace Engineering, Case Western Reserve University, Cleveland, Ohio 44106, U.S.A.

0195-928X/02/0500-0649/0 © 2002 Plenum Publishing Corporation

1. INTRODUCTION

During liquid self-diffusion experiments, a small non-uniformity in temperature within the melt may drive a buoyant convection in the presence of gravity (terrestrial experiments) or even with residual acceleration magnitudes characteristic of microgravity conditions. This convection can result in erroneous values of the measured diffusivity. Verhoeven [1] emphasized that any horizontal component of a density gradient in the liquid results in spontaneous convection with no threshold. Since in most practical situations, particularly at high temperatures where the presence of a horizontal temperature gradient is difficult to avoid, it has been a widespread practice to keep the top wall of diffusion capillaries slightly warmer than the bottom wall to produce a so-called "stabilizing" temperature gradient that might reduce the magnitude of flow velocities caused by horizontal density gradients.

Alexander et al. [2] showed that for three-dimensional (3D) time-dependent transport in the presence of gravity with horizontal temperature non-uniformities across the sample as low as 1 and 0.1 K, convective transport rates in 1 and 3 mm diameter capillaries, respectively, can exceed diffusive transport rates, and, thus, result in higher values of measured diffusivities. Also, the addition of the top-warmer "stabilizing" temperature gradient actually increased the overall transport in self-diffusion experiments. Alexander and Banish [3] have presented the results of a combination of numerical modeling and order-of-magnitude estimates of the sensitivity of convective contamination to microgravity and low-gravity of self-diffusion coefficient experiments.

Recently, some researchers [4–6] have applied magnetic fields to suppress the buoyant convection in the liquid metals and semiconductors since they have very large electrical conductivities. Youdelis et al. [7] discussed that at high magnetic field strengths, the diffusion process itself can be significantly modified through the Lorentz body force acting on the ions and electrons in the conducting liquids. Alboussiere et al. [8] found that with Lorentz electromagnetic damping of convection and with resulting reduced convection levels, the convective contribution to the effective mass Péclet number is scaled as Hartmann number Ha^{-4}.

In actual self-diffusivity experiments, measured diffusivity results that deviate by less than 5% from the (known) real value, D_0, would be considered "acceptable" though not ideal. In self-diffusion experiments, temperature gradients drive the buoyant convection responsible for erroneous diffusivity measurements. The purpose of this paper is to quantitatively estimate the magnitude of allowable temperature non-uniformities in the liquid that will guarantee that measured diffusivity values lie within 5% of

the actual value when the experimental system is subject to an axial magnetic field. To model the experiment, axisymmetric, time-dependent transport due to a combination of steady flow and diffusion is considered.

In this basic model, a steady, uniform heat flux that produces a radial temperature difference in the liquid is imposed on the sidewall of the cylindrical container while uniform heat losses are imposed on the top and bottom walls. Then, a steady, spatially-periodic heat flux is superimposed on the sidewall of the cylinder to predict the effect of spatial temperature variations which represent the localized hot and cold spots along the sidewall. Note that the overall flux for this additional periodic condition is zero. Simulated diffusivity results for two different initial conditions with two different magnetic field strengths and five various temperature profiles along the sidewall are presented in this paper. The effect of a top wall slightly warmer than the bottom wall is also discussed.

2. PROBLEM FORMULATION

In this model, the liquid is assumed to be a Boussinesq fluid contained in a closed vertical circular cylinder of length $Z = 30$ mm with an inside radius R of 1.5 mm. Gravity acts downward along the cylinder axis while a uniform axial magnetic field is applied in the opposite direction as in Fig. 1a. The origin lies at the centerline ($R = 0$) and $z = Z/(2r)$. The isopicnic radioactive tracer is at the bottom of the cylinder at the beginning of the measurements. The dimensionless model has the top and bottom limits of $z = 10$ and -10, respectively, while the vertical wall lies at $r = 1$.

2.1. Thermal Problem

For sufficiently large values of magnetic field strength B, the magnetic damping results in a characteristic ratio of convective to conductive heat transfer (the thermal Péclet number, $Pe = \rho c_h U R/\lambda$, where ρ is uniform density, c_h is the specific heat, U is a characteristic velocity, and λ is the thermal conductivity) is small; the dimensionless temperature in this case is then governed by $\nabla^2 T = 0$. Therefore, in this model, we assume that convective heat transfer is negligible (i.e., $Pe \ll 1$) and that a uniform heat flux density is imposed along the vertical wall and constant heat losses through the top and bottom walls of the cylinder with the possibility of an additional spatially-periodic heat flux of various amplitude and wavelength on the vertical sidewall in some cases. With these assumptions, the energy equation ($\nabla^2 T = 0$) is non-dimensionalized by R for length and $2\Delta T_r$ for temperature, where ΔT_r is the temperature difference between the centerline

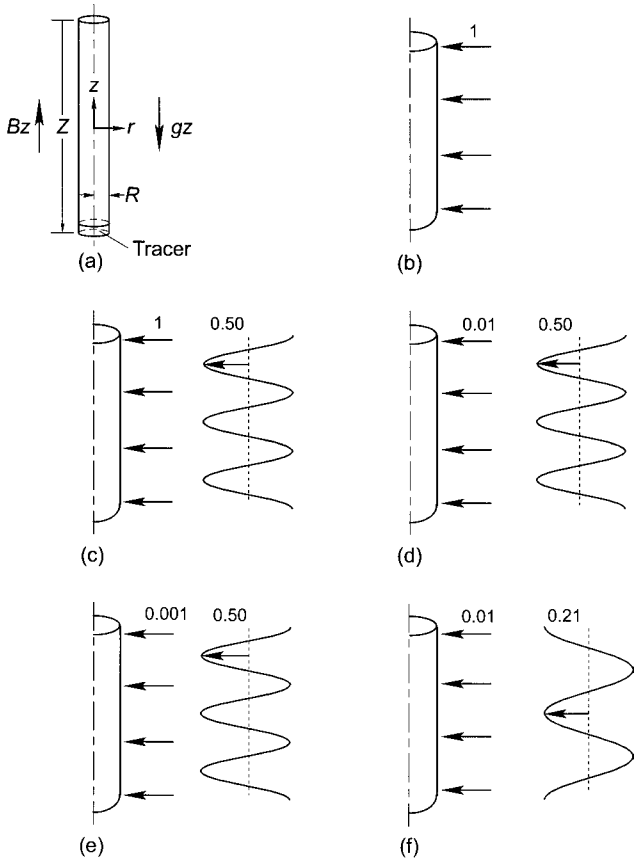

Fig. 1. Model diffusion capillary. Figure 1a presents the set up and Figs. 1b–1f describe the dimensionless incoming heat fluxes for Cases I through V.

and the vertical (side) wall and the dimensionless analytical solution for temperature is

$$T(r, z) = s_1 \left(\frac{r^2}{2} - z^2 \right) + s_2 I_0(ar) \cos(az) \tag{1}$$

where $a = n\pi/10$ and n is a known integer, s_1 and s_2 are set coefficients, and I_0 is a modified Bessel function of the first kind of order zero. The first term on the right hand side of Eq. (1) represents the temperature distribution due to a uniform heat flux while the second term represents the temperature distribution due to a spatially-periodic heat flux.

2.2. Flow Problem

At sufficiently large values of B, the characteristic ratio of the electromagnetic body force to the inertial effect (the interaction parameter, $N = \sigma B^2 R/(\rho U)$, where σ is the electrical conductivity of the liquid) is very large and, thus, the inertial terms in the Navier–Stokes equations become negligible. In addition to the applied magnetic field produced by the magnet, associated electric currents induce an additional magnetic field since the materials considered here are electrically conducting. The characteristic ratio of the induced to applied magnetic field strengths is the magnetic Reynolds number, $R_m = \mu_p \sigma U R$, (where μ_p is the magnetic permeability of the liquid) and this is very small for crystal growth processes and self-diffusion experiments of liquid metals and semiconductors. Thus, neglect of the induced magnetic field effect is justifiable in the model presented here.

Khine and Walker [9] determined the characteristic velocity for magnetically damped axisymmetric buoyant convection $U = 2\rho g_0 \beta \Delta T_r/(\sigma B^2)$, where g_0 is the gravitational acceleration ($9.81\ \mathrm{m \cdot s^{-2}}$) and β is the volumetric expansion coefficient for Boussinesq approximation, and this is used to non-dimensionlize the velocity. The magnetic flux, reduced pressure (the difference between the total pressure and the hydrostatic pressure) with uniform density, the electric current density, and the electric potential are non-dimensionalized using B, $\sigma U B^2 R$, $\sigma U B$, and UBR, respectively. The dimensionless, inertialess equations governing the steady, axisymmetric buoyant convection are then

$$\nabla \cdot \mathbf{v} = 0 \tag{2a}$$

$$\nabla p = T\hat{z} + \mathbf{j} \times \hat{z} + Ha^{-2} \nabla^2 \mathbf{v} \tag{2b}$$

$$\nabla \cdot \mathbf{j} = 0 \tag{2c}$$

$$\mathbf{j} = -\nabla \phi + \mathbf{v} \times \hat{z} \tag{2d}$$

Here, $Ha = BR(\sigma/\mu)^{1/2}$, where μ is the viscosity of the liquid, Eq. (2a) is the conservation of mass, Eq. (2b) is the Navier–Stokes equation with a buoyancy force and an electromagnetic body force, Eq. (2c) is the continuity of electric current density $\mathbf{j}$, and Eq. (2d) is Ohm's law with an electric potential function ϕ. Cross-differentiating the r and z components of Eq. (2b) to eliminate pressure p, and introducing a stream function, $\psi(r,z)$ which satisfies Eq. (2a), yields

$$v_r = \frac{1}{r} \frac{\partial \psi}{\partial z} \tag{3a}$$

$$v_z = -\frac{1}{r} \frac{\partial \psi}{\partial r} \tag{3b}$$

Using Eqs. (3a) and (3b), the equation governing ψ for a composite core-parallel layer solution where the axial derivative of the stream function is much smaller compared to the radial derivatives in the viscous dissipation becomes

$$Ha^{-2}\left\{\frac{\partial^4\psi}{\partial r^4}-\frac{2}{r}\frac{\partial^3\psi}{\partial r^3}+\frac{3}{r^2}\frac{\partial^2\psi}{\partial r^2}-\frac{3}{r^3}\frac{\partial\psi}{\partial r}\right\}-\frac{\partial^2\psi}{\partial z^2}=s_1r^2+s_2arI_1(ar)\cos(az) \tag{4a}$$

after being multiplied with r where I_1 is the modified Bessel function of the first kind of order one. Here, the terms multiplied with Ha^{-2} represent the viscous dissipation of the azimuthal vorticity, $\frac{\partial^2\psi}{\partial z^2}$ is the electromagnetic suppression of this vorticity, and the terms on the right side are the production of this vorticity due to the rotational part of the buoyancy force. The boundary conditions are

$$\psi=\frac{\partial\psi}{\partial r}=0, \qquad \text{at} \quad r=1 \tag{4b}$$

$$\psi=0, \qquad \text{at} \quad z=-10,\,10 \tag{4c}$$

Condition (Eq. (4b)) is simplified by multiplying with $(1-z^2)^{-1/2}\,T_{2P}(z/10)$ where T_{2P} is the even Chebyshev polynomial and by integrating from $z=0$ to 10. Since the Chebyshev polynomials are orthogonal, the only term remaining in the sum of M is the term for $P=M$ where P and M are numbers of terms in Chebyshev polynomials in z. For various values of Ha, Eq. (3) is solved using a Chebyshev spectral collocation method [10] where the collocation points are at $r=\cos[I\pi/(2N_R)]$ and $z=\cos[K\pi/(2N_Z)]$, where I and K are indices for collocation points in r and z, respectively, and N_R and N_Z are total number of collocation points in r and z, respectively. In this case, ψ is defined as even functions of Chebyshev polynomials in r and z.

$$\psi(r,z)=r^2\sum_{L=0}^{N_R}\sum_{M=0}^{N_Z}A_{LM}T_{2L}(r)\,T_{2M}\left(\frac{z}{10}\right), \qquad \text{for} \quad 0<r\leqslant 1, \quad 0\leqslant z\leqslant 10 \tag{5}$$

Here, A_{LM} are unknown coefficients of ψ and T_{2L} and T_{2M} are even Chebyshev polynomials in r and z, respectively.

2.3. Diffusion Problem

The dimensionless axisymmetric governing equation for diffusion is

$$\frac{\partial c}{\partial t}+Pe_m\mathbf{v}\cdot\nabla c=\nabla^2c \tag{6a}$$

Here, t is normalized by the diffusion time scale (R^2/D_0) and c is scaled by the initial concentration C_0. The first term on the left side of Eq. (6a) is the rate of change of concentration with time, the second term represents the mass transport due to convective effects while $\nabla^2 c$, on the right side, represents pure diffusion. $Pe_m = UR/D_0$ is the characteristic ratio of convective effects to diffusive effects in the process. Here, U is the calculated characteristic velocity and differs from case to case. Since there is no mass transfer across any boundary, the boundary conditions are

$$\frac{\partial c}{\partial r} = 0, \qquad \text{at} \quad r = 1 \tag{6b}$$

$$\frac{\partial c}{\partial z} = 0, \qquad \text{at} \quad z = -10,10 \tag{6c}$$

Equation (6a) is solved for different Pe_m with conditions (6b, 6c) using a Chebyshev spectral collocation method for spatial discretization as in the flow problem while conventional finite-difference is used for temporal discretization. Equation (6) is cast into $\mathbf{M1} * D_{LM}(t+\Delta t) = \mathbf{M2} * D_{LM}(t)$ where **M1** and **M2** are time independent matrices which consist of flow variables and Chebyshev polynomials and D_{LM} are unknown coefficients of c. In this case, the concentration c is defined in terms of Chebyshev polynomials as

$$c(r, z, t) = \sum_{L=0}^{N_R} \sum_{M=0}^{2*N_Z} D_{LM}(t)\, T_{2L}(r)\, T_M\left(\frac{z}{10}\right) \tag{7}$$

Note that, in self-diffusion of a single-component system, the liquid density is independent of the "tracer" concentration, and thus, the equations of motion, Eqs. (4), need not be solved simultaneously with the diffusion equation, Eq. (6). We first solve for the velocity field and then use the results in Eq. (6) which greatly simplifies the computations with no loss of accuracy.

In this paper, two initial conditions for c are considered where both are common practices in self-diffusion experiments. The first one is that the tracer forms a thin layer at the bottom of the cylinder, and it is represented by

$$c(r, z, t = 0) = \exp(-\alpha(z+10)^2) \tag{8a}$$

where $\alpha = 3$ and dramatically to $c \approx 0$ around $z = -9$.

The second initial condition is that the tracer occupies one half of the cylinder which is represented by

$$c(r, z, t=0) = 0.5 * [1 - \tanh(\alpha z)] \tag{8b}$$

where $\alpha = 10$. This initial condition gives $c = 1$ for $z = -10$ to $z < 0$, $c = 0.5$ at $z = 0$, and then decreases dramatically to $c = 0$ for $z > 0$.

The simulated measurements (or output diffusivities D) are computed from the resulting time traces of concentration through a straight line fit in the form,

$$\ln[c_1(t) - c_2(t)] = \text{constant} - \left(\frac{\pi^2 D}{Z^2}\right) t \tag{9}$$

which is known as Codastefano [11] or Harned [12] technique. Here, c_1 and c_2 are located at $z = Z/6$ and $5Z/6$ along the length of the cylinder, respectively, and the *constant* depends on the concentration profile $c(z)$ at $t = 0$ and it does not enter explicitly into the D-evaluation. This methodology has been refined in our laboratory through extensive experimental and numerical modeling [3, 13–16].

Only the region between $z = 0$ and 10 is considered in the flow problem due to symmetry at $z = 0$. Fifteen collocation points are needed in the radial direction while 40 points are used in axial direction. In the diffusion problem, the total number of collocation points in r is 15 and that in z is 80 since the entire cylinder is considered. Liquid indium with $\beta = 1.02 \times 10^{-4}\ \mathrm{K}^{-1}$, $\rho = 6.64 \times 10^3\ \mathrm{kg \cdot m^{-3}}$ and $\sigma = 3.02 \times 10^6\ \mathrm{S \cdot m^{-1}}$ [17] is used as a model fluid. A time step size of 0.1 or 0.2 was used for time integration, and several different Pe_m are considered for each Ha. A self-diffusivity value of $D_0 = 1.48 \times 10^{-5}\ \mathrm{cm^2 \cdot s^{-1}}$ was used as the input. Two different Hartmann numbers are considered. For liquid indium these correspond to magnetic field strengths of 0.218 T ($Ha = 25$) and 0.873 T ($Ha = 100$).

The numerical model was verified by considering an analytical solution at high Ha where the viscous effect is neglected, and the two results agree very well. Also, the diffusion results are verified by checking the total tracer concentration in the cylinder at certain time steps.

3. RESULTS AND DISCUSSION

The results for five different incoming heat fluxes (see Figs. 1b to 1f) are presented in this section. Case I presents self-diffusion with a radial temperature difference only as the driving force in the liquid due to the steady, uniform heat flux along the sidewall. Cases II through V present

self-diffusion with various magnitude of uniform heat flux and superimposed, steady, spatially-periodic heat flux with various amplitude and wavelength along the sidewall (i.e., localized hot and cold spots along the sidewall in addition to the radial temperature difference in the liquid). The desired incoming heat fluxes for Cases I through V are obtained by adjusting s_1, s_2 and a in Eq. (1). Table I presents summarized results for those five different cases.

Case I. $s_1 = 1$ *and* $s_2 = 0$ *in Eq. (1)*

In this case, a uniform heat flux of density 1 that produces a radial temperature difference in the liquid is applied through the vertical wall with uniform heat loss through the top and bottom end walls as in Fig. 1b. The isotherms show symmetry from $z = 0$ plane, and are slightly deviated from the horizontal, and decrease toward the top and bottom walls. The streamlines for both *Ha* circulate in counterclockwise motion beginning near the vertical wall.

To illustrate typical flow geometries, Figs. 2 and 3 show contours of the radial velocity component v_r and axial velocity component v_z for $Ha = 100$ ($B = 0.873$ T). v_r is equal in magnitude and opposite in direction with a mid-plane at approximately $z = 0$. The maximum and minimum values of v_r are 2.89 near the bottom wall and -2.89 near the top wall, respectively. In Fig. 3, v_z increases from the centerline toward the vertical wall while $v_z = 0$ occurs near $r = 0.6$. The maximum v_z is 27.2 and occurs near the vertical wall, and the minimum value is –75.8 and occurs near the origin. Increasing the magnetic field, from 0.218 to 0.873 T, causes the single convection cell to be squeezed towards the center of circulation. $|v_{r\max}|/|v_{z\max}|$ decreases from 0.114 to 0.038 for Case I. A similar effect is seen for Case II (below) where there is again only a single flow cell. For the other three cases, which have multiple stacked cells (Cases III, IV, and V have 5, 5, and 3 cells, respectively) this ratio stays essentially the same as the magnetic field increases.

These dimensionless velocity results are multiplied with the corresponding characteristic velocity U for a particular Pe_m in order to obtain the dimensional velocities of interested Pe_m. Some important results for Cases I through V are included in Table I. Given a known *Ha* (magnetic field strength) and a Pe_m (rate of convective to diffusive transport), one can determine the negligible temperature non-uniformity for that particular set of *Ha* and Pe_m, or *vice versa*, from Table I.

Both initial conditions (Eqs. (8a) and (8b)) where the tracer forms a thin layer and the tracer occupies one half of the cylinder, respectively, were used in separate calculations for $Ha = 25$ and 100. The characteristic diffusion time is 1520 s, and, accordingly, values of Pe_m between 0 and 4

Table I. Summary of Results for Cases I to V

ΔT_r (K)	$\lvert v_{r\,\max}\rvert$ (cm·s^{-1})	$\lvert v_{z\,\max}\rvert$ (cm·s^{-1})	U (cm·s^{-1})	effective Pe_m	$D \times 10^5$ (cm^2·s^{-1})
Case I. $s_1 = 1$ and $s_2 = 0$ in Eq. (1)					
$B = 0.218$ T, $Ha = 25$					
0.00107	7.34×10^{-6}	6.42×10^{-5}	9.87×10^{-6}	0.651	1.49
0.00373	$\mathbf{2.57 \times 10^{-5}}$	$\mathbf{2.25 \times 10^{-4}}$	$\mathbf{3.46 \times 10^{-5}}$	**2.28**	**1.55**
0.0107	7.34×10^{-5}	6.42×10^{-4}	9.87×10^{-5}	6.51	1.99
0.0426	2.94×10^{-4}	2.57×10^{-3}	3.95×10^{-4}	26.04	9.57
$B = 0.873$ T, $Ha = 100$					
0.00171	2.85×10^{-6}	7.48×10^{-5}	9.87×10^{-7}	0.758	1.49
0.00501	$\mathbf{8.35 \times 10^{-6}}$	$\mathbf{2.19 \times 10^{-4}}$	$\mathbf{2.89 \times 10^{-6}}$	**2.22**	**1.55**
0.0171	2.85×10^{-5}	7.48×10^{-4}	9.87×10^{-6}	7.58	2.11
0.0854	1.43×10^{-4}	3.74×10^{-3}	4.93×10^{-5}	37.9	16.0
Case II. $s_1 = s_2 = 1$ and $n = 3$ in Eq. (1)					
$B = 0.218$ T, $Ha = 25$					
0.00107	5.92×10^{-6}	7.56×10^{-5}	9.87×10^{-6}	0.766	1.49
0.00373	$\mathbf{2.07 \times 10^{-5}}$	$\mathbf{2.65 \times 10^{-4}}$	$\mathbf{3.45 \times 10^{-5}}$	**2.68**	**1.55**
0.0107	5.92×10^{-5}	7.56×10^{-4}	9.87×10^{-5}	7.66	1.99
$B = 0.873$ T, $Ha = 100$					
0.00171	2.83×10^{-6}	7.64×10^{-5}	9.87×10^{-7}	0.774	1.49
0.00548	$\mathbf{9.07 \times 10^{-6}}$	$\mathbf{2.45 \times 10^{-4}}$	$\mathbf{3.16 \times 10^{-6}}$	**2.48**	**1.55**
0.0171	2.83×10^{-5}	7.64×10^{-4}	9.87×10^{-6}	7.74	2.12
Case III. $s_1 = 0.01$, $s_2 = 1$, and $n = 3$ in Eq. (1)					
$B = 0.218$ T, $Ha = 25$					
0.00533	8.78×10^{-6}	6.41×10^{-5}	4.93×10^{-5}	0.652	1.49
0.0249	$\mathbf{4.11 \times 10^{-5}}$	$\mathbf{3.00 \times 10^{-4}}$	$\mathbf{2.31 \times 10^{-4}}$	**3.04**	**1.55**
0.0639	1.05×10^{-4}	7.70×10^{-4}	5.92×10^{-4}	7.82	1.84
$B = 0.873$ T, $Ha = 100$					
0.0427	8.46×10^{-6}	6.04×10^{-5}	2.47×10^{-5}	0.612	1.49
0.171	$\mathbf{3.38 \times 10^{-5}}$	$\mathbf{2.42 \times 10^{-4}}$	$\mathbf{9.87 \times 10^{-5}}$	**2.45**	**1.55**
0.684	1.35×10^{-4}	9.67×10^{-4}	3.95×10^{-4}	9.79	2.2
Case IV. $s_1 = 0.001$, $s_2 = 1$, and $n = 3$ in Eq. (1)					
$B = 0.218$ T, $Ha = 25$					
0.00533	8.78×10^{-6}	6.17×10^{-5}	4.93×10^{-5}	0.624	1.49
0.0262	$\mathbf{4.31 \times 10^{-5}}$	$\mathbf{3.03 \times 10^{-4}}$	$\mathbf{2.42 \times 10^{-4}}$	**3.07**	**1.55**
0.0639	1.05×10^{-4}	7.40×10^{-4}	5.92×10^{-4}	7.50	1.84

Table I. *(Continued)*

ΔT_r (K)	$\lvert v_{r\,\max}\rvert$ (cm·s^{-1})	$\lvert v_{z\,\max}\rvert$ (cm·s^{-1})	U (cm·s^{-1})	effective Pe_m	$D \times 10^5$ (cm^2·s^{-1})
		$B = 0.873$ T, $Ha = 100$			
0.0427	8.61×10^{-6}	5.06×10^{-5}	2.47×10^{-5}	0.513	1.49
0.184	$\mathbf{3.71 \times 10^{-5}}$	$\mathbf{2.18 \times 10^{-4}}$	$\mathbf{1.06 \times 10^{-4}}$	**2.21**	**1.55**
0.513	1.03×10^{-4}	6.07×10^{-4}	2.96×10^{-4}	6.15	1.87
		Case V. $s_1 = 0.01$, $s_2 = 1$, and $n = 2$ in Eq. (1)			
		$B = 0.218$ T, $Ha = 25$			
0.0107	1.04×10^{-5}	8.39×10^{-5}	9.87×10^{-5}	0.850	1.49
0.0426	$\mathbf{4.14 \times 10^{-5}}$	$\mathbf{3.35 \times 10^{-4}}$	$\mathbf{3.95 \times 10^{-4}}$	**3.40**	**1.55**
0.107	1.04×10^{-4}	8.39×10^{-4}	9.87×10^{-4}	8.50	1.86
		$B = 0.873$ T, $Ha = 100$			
0.0854	1.00×10^{-5}	6.91×10^{-5}	4.93×10^{-5}	0.700	1.49
0.222	$\mathbf{2.60 \times 10^{-5}}$	$\mathbf{1.80 \times 10^{-4}}$	$\mathbf{1.28 \times 10^{-4}}$	**1.82**	**1.55**
0.854	1.00×10^{-4}	6.91×10^{-4}	4.93×10^{-4}	7.00	2.26

are considered here. At $t = 0.1$ (i.e., 152 s in real time) for $Ha = 25$ and the initial condition Eq. (8a), the radial average concentration curves for $Ha = 25$ and various Pe_m are indistinguishable. At $t = 1$, the results for $Pe_m > 1$ begin to show a faster evolution of the concentration profile than for $Pe_m < 1$. Figure 4 presents the radial average concentration at $t = 10$ for various Pe_m. As one would intuitively expect, for $Pe_m < 1$, the $c(z)$

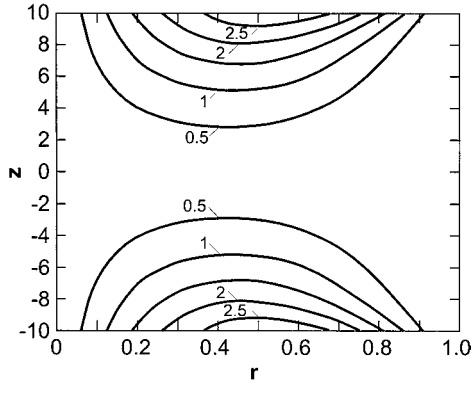

Fig. 2. Contours of v_r for Case I: $Ha = 100$; maximum $v_r = 2.89$; minimum $v_r = -2.89$.

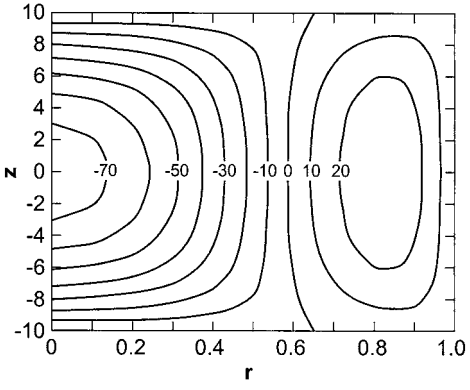

Fig. 3. Contours of v_z for Case I: $Ha = 100$; maximum $v_z = 27.2$; minimum $v_z = -75.8$.

plots are nearly identical. In contrast, the contours for $Pe_m = 4$ are almost fully diffused. Thus, we see the effect of convective contamination on diffusivity measurements. At $t = 100$, the $Pe_m = 2$ curve shows essentially uniform $c(z)$.

For $Ha = 100$ with the initial condition (Eq. (8a)), the radial average concentration curves for $Pe_m > 1$ show a faster decay rate (and, thus, will yield a higher measured diffusivity) than the curves corresponding to

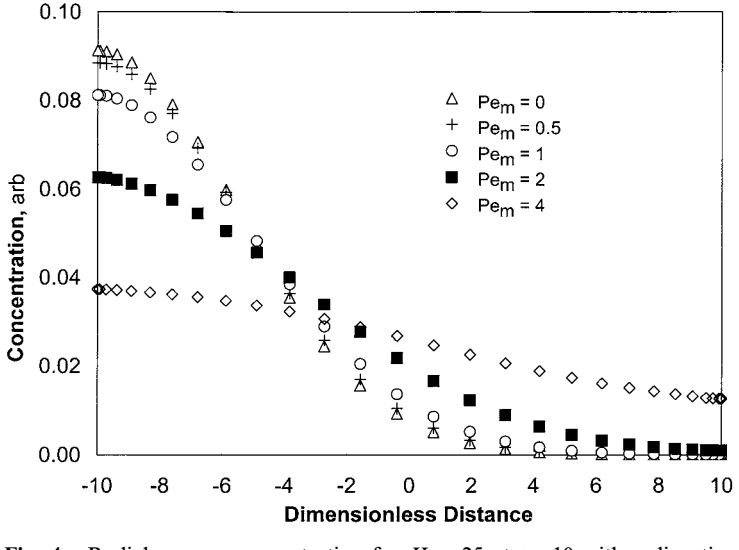

Fig. 4. Radial average concentration for $Ha = 25$ at $t = 10$ with radioactive tracer at the bottom of cylinder at $t = 0$.

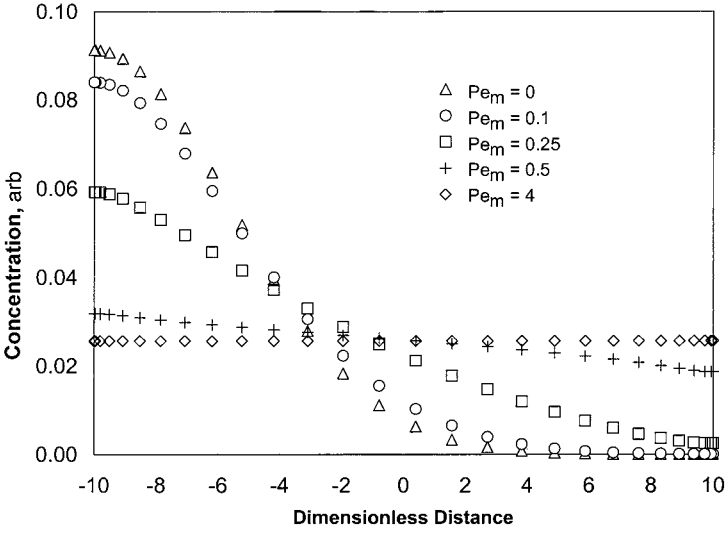

Fig. 5. Radial average concentration for $Ha = 100$ at $t = 10$ with radioactive tracer at the bottom of cylinder at $t = 0$.

$Pe_m < 1$ at $t = 0.1$. At $t = 2$, both $Pe_m = 2$ and 4 curves are at steady state while the $Pe_m = 1$ curve is approaching to steady state. Figure 5 presents the radial average concentration at $t = 10$ for $Ha = 100$ with initial condition (8a). Here, the radial average concentration curves for $Pe_m = 1, 2$, and 4 are at steady state while $Pe_m = 0.5$ is approaching to steady state while the rest are still decaying. At $t = 100$, the results for $Pe_m < 0.1$ are still decaying while the rest are at steady state.

Both initial conditions, Eqs. (8a) and (8b), give the same diffusivity results for both *Ha*'s and the various Pe_m. In each case, the effect of convection is quite obvious by considering the effective Pe_m, which is $Pe_m\,|v_{\max}|$. Figure 6 presents the diffusivity vs. effective Pe_m for $Ha = 25$ and 100. For both *Ha*, the results lie on one curve that bows upward as the effective Pe_m increases. From the results, we can see that the convective effect is extremely large for a larger effective Pe_m. For effective $Pe_m < 2$, the predicted convective effect in self-diffusivity measurements (i.e., difference in diffusivity from D_0) is less than 5% for both $Ha = 25$ and 100. The allowable driving force ΔT_r for $Ha = 25$ is about 0.00373 K while that for $Ha = 100$ is about 0.00501 K to prevent convective contamination in excess of 5%.

Case II. $s_1 = s_2 = 1$ *and* $n = 3$ *in Eq. (1)*

In this case, the uniform heat flux is the same as in Case I which produces a radial temperature difference in the liquid while a periodic flux

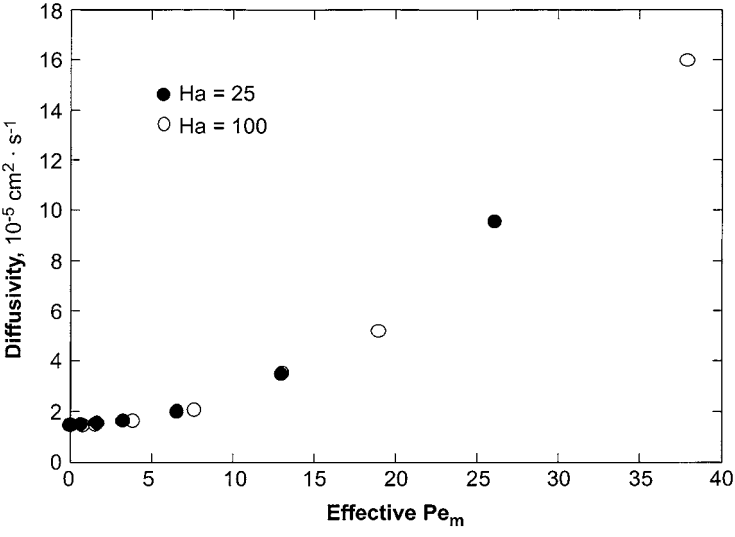

Fig. 6. Diffusivity vs. effective Pe_m for Case I.

with an amplitude of 0.495 is superimposed at the sidewall to produce the localized periodic temperature variation effect. Here, $n = 3$ represents the number of periodicity in the non-uniform heat flux. The maxima of the periodic flux occur at $z = -6.67$, 0 (mid-plane), and 6.67 while the minima occur at $z = -10$ (bottom wall), -3.33, 3.33, and 10 (top wall). So, the top and bottom walls, $z = Z/6$ and $5Z/6$ are slightly cooler than the rest of the cylinder. The isotherms in this case are similar to those in Case I.

The patterns of flow for both *Ha* are similar to those in Fig. 2 except the contours have a distinct axial waviness due to the presence of periodic temperature at the sidewall. For Case II, the diffusivity results are plotted in Fig. 7 for both values of *Ha*. Again, the two curves bow upward as the effective Pe_m increases. The curve for $Ha = 100$ is slightly higher than that for $Ha = 25$. The difference is more obvious at a larger effective Pe_m. For the diffusivity results of less than 5% deviation from D_0, the allowable ΔT_r for $Ha = 25$ is 0.00373 K and that for $Ha = 100$ is 0.00548 K. Case II results are very close to those of Case I. The spatially-periodic temperature along the sidewall does not affect the diffusivities significantly although the presence is observed in the flow pattern.

Case III. $s_1 = 0.01$, $s_2 = 1$, *and* $n = 3$ *in Eq. (1)*

As shown in Fig. 1d, the uniform heat flux with a magnitude of 0.01 (i.e., 100 times smaller than that in Case I) and a spatially-periodic flux with an amplitude of 0.495 (same as in Case II) are imposed at the sidewall.

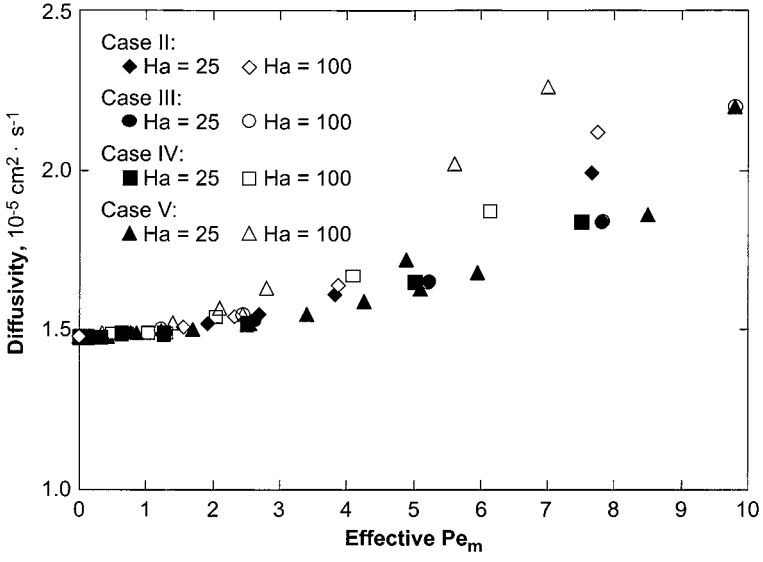

Fig. 7. Diffusivity vs. effective Pe_m for Cases II, III, IV and V.

In other words, the radial temperature difference in the liquid is reduced 100 times while keeping the superimposed periodic temperature profile unchanged. The isotherms show symmetry from $z = 0$ plane, and are deviated slightly from the horizontal. The streamlines for both $Ha = 25$ and 100 are arranged as 5 vertically stacked cells with a counterclockwise circulation at the top wall. The maximum dimensional radial and axial velocities for some Pe_m are presented in Table I along with corresponding diffusivities.

For Case III, the consequences of the magnetic field for transport can be seen from the diffusivity vs. the effective Pe_m shown in Fig. 7. For both Ha, the curves bow upward as the effective Pe_m increases. The effect of convection on the measured diffusivity is more prominent at a larger effective Pe_m. Also, the diffusivity curve for $Ha = 100$ lies above the curve for $Ha = 25$. For less than 5% deviation from D_0, the driving ΔT_r for $Ha = 25$ is about 0.0249 K while for $Ha = 100$, it is 0.171 K. Thus, Case III suggests that reducing the radial temperature gradient in the liquid by 100 times from its original value (as in Case I) has a tremendous effect on the diffusivity results for this model. The effect is more prominent at higher Ha for this case (i.e., at stronger magnetic field strength).

Case IV. $s_1 = 0.001$, $s_2 = 1$, *and* $n = 3$ *in Eq. (1)*

Here, the uniform heat flux which produces a radial temperature difference in the liquid is further reduced to a magnitude of 0.001 (i.e.,

10 times less than that in Case III and 1000 times less than that in Case I) while keeping the periodic temperature profile unchanged as in Cases II and III. For both *Ha*, the streamlines form five cells between the top and bottom walls. The diffusivity vs. effective Pe_m for Case IV is shown in Fig. 7 for both *Ha*. As in the previous case, the two curves bow upward as the effective Pe_m increases, and the curve for $Ha = 100$ is higher than that for $Ha = 25$, especially at larger effective Pe_m. The allowable ΔT_r in this case for $Ha = 25$ is 0.0262 K while that for $Ha = 100$ is 0.184 K which is a slight improvement from those in Case III. Thus, reducing the magnitude of radial temperature gradient by 10 times from Case III does not result in tremendous changes in diffusivity results.

Case V. $s_1 = 0.01$, $s_2 = 1$, *and* $n = 2$ *in Eq. (1)*

This case is the same as Case III except $n = 2$ here so that the isotherms decrease and increase two times alternatively in between the top and bottom walls (i.e., the periodicity is 2 here). The uniform flux which produces the radial temperature difference is 100 time smaller than that in Case I. The maxima of spatially-periodic flux occur at $z = -10$ (bottom wall), 0 (mid-plane), and 10 (top wall) with a magnitude of 0.207 while the minima occur at $z = -5$ and 5. So, the top and bottom walls and the mid-plane are slightly warmer than the rest of the cylinder.

For $Ha = 100$, there are three negative and positive circulations. The diffusivities vs. effective Pe_m for Case V are plotted in Fig. 7 for both *Ha*. The curve for $Ha = 100$ is higher than that for $Ha = 25$ and the convective effects are more obvious at larger effective Pe_m. In this case, the allowable temperature non-uniformity ΔT_r for $Ha = 25$ is 0.0426 K and that for $Ha = 100$ is 0.222 K. The results are close to those of Case III with an improvement in sensitivity of allowable temperature for the same magnetic field strength.

Since keeping the top wall of diffusion capillary slightly warmer than the bottom wall is a common way to reduce the convection from the horizontal density gradients, the effect of ΔT_z in addition to ΔT_r is considered in this paper. Without an applied magnetic field, an axial temperature difference leads to radial temperature gradients through the convection of high and low temperatures with the upward and downward flows, which suggest that convective heat transfer is not negligible in the problem. However, with an applied magnetic field, the effective Pe_m for our model results in $Pe < 0.026$ for $Ha = 25$ and $Pe < 0.303$ for $Ha = 100$ for the temperature distribution in Eq. (1). These small values of *Pe* suggest that convective heat transfer is negligible in the energy equation and thus such assumption in the thermal problem of our model is verified. Therefore, for the simple cases described here, keeping the top wall warmer than the

bottom wall has no effect on the measured diffusivity. This is because the buoyant convection in this case is driven only by radial gradients, that in the case examined here, are not changed significantly. In fact, in some cases they may be enhanced or diminished, depending on the explicit nature of the actual heat transfer conditions.

4. CONCLUSIONS

The use of an axial magnetic field to offset the detrimental effects of convection on diffusivity measurements in liquid metals has been examined using a numerical model. Our goal was to determine what magnetic field strengths would be necessary given various temperature non-uniformities to ensure that convective transport was less than 5% of the diffusive. Two different flow patterns were observed for the various imposed temperature non-uniformities. For a uniform heat flux along the sidewall that produces a radial temperature difference in the liquid, the streamlines form a counterclockwise motion. For a spatially-periodic heat flux which produces the localized hot and cold spots on the vertical wall, the flow is arranged as vertically stacked cells and the number of cells depends on the periodicity of the temperature profile due to periodic flux.

In all cases, the value of the simulated diffusivity increased with increasing effective Pe_m (i.e., with increasing temperature difference, and, thus, convective velocity magnitude). The dependence of the transport conditions on the nature of the thermal boundary conditions was such that for a uniform heat flux along the sidewall which produces a radial temperature difference in the liquid, the diffusivity vs. Pe_m were indistinguishable for $Ha = 25$ and 100. The diffusivities for $Ha = 100$ were higher than those for $Ha = 25$ in the presence of a periodic temperature profile produced by a periodic heat flux superimposed on a uniform heat flux (Cases II, III, IV, and V). For $Ha = 25$, the allowable temperature non-uniformities ΔT_r for Cases I through V range from 0.00373 to 0.0426 K, and that for $Ha = 100$ ranges from 0.00501 to 0.222 K.

Case I which is uniform heat flux only (i.e., the radial temperature difference in the liquid is the only driving force) seems to be the most sensitive while Case V (when the uniform heat flux that produces radial temperature difference in the liquid is reduced 100 times that of Case I and the periodic temperature profile produced by a non-uniform flux with the periodicity of 2 is superimposed) is the least sensitive among five different conditions considered in this model. From the results, one can conclude that a particular temperature profile at the sidewall (produced by a combination of uniform and non-uniform heat fluxes) is required to result in desired diffusivities (i.e., to operate within the allowable temperature

non-uniformities) in self-diffusion experiments for this numerical model. For a fixed value of effective Pe_m, ΔT_r increases with increasing Ha (the magnetic field strength). Thus, stronger magnetic fields can tolerate a stronger driving force ΔT_r in self-diffusivity measurements for same convective conditions. Keeping the top wall of the cylinder warmer than the bottom wall was found to have no effect on the convective contamination during the self-diffusivity measurements for this model.

ACKNOWLEDGMENTS

The support by National Aeronautics and Space Administration through Grants NCC8-99 and NAG8-1476 for this research is gratefully acknowledged. We are very thankful to Professor J. S. Walker at University of Illinois at Urbana-Champaign for his suggestions and help. Thanks also go to Lynne Carver for preparation of figures.

REFERENCES

1. J. D. Verhoeven, *Trans. Met. Soc. AIME* **242**:1937 (1968).
2. J. I. D. Alexander, J.-F. Ramus, and F. Rosenberger, *Microgravity Sci. Tech.* **9**:158 (1996).
3. J. I. D. Alexander and R. M. Banish, *Microgravity Sci. Tech.* **11**:90 (1998).
4. L. N. Hjellming and J. S. Walker, *J. Fluid Mech.* **164**:237 (1986).
5. N. Ma and J. S. Walker, *Phys. Fluids.* **9**:1182 (1997).
6. N. Ma, K. O. Homan, and J. S. Walker, *Phys. Fluids.* **9**:2789 (1997).
7. W. V. Youdelis, D. R. Colton, and J. Cahoon, *Can. J. Phys.* **42**:2217 (1964).
8. T. Alboussiere, J. P. Garandet, P. Lehmann, and R. Moreau, *Fluid Mechanics and its Applications: Transfer Phenomena in Magnetohydrodynamic and Electroconducting Flows*, Vol. 51 (Kluwer, New York, 1999), pp. 359–372.
9. Y. Y. Khine and J. S. Walker, *J. Crystal Growth* **147**:313 (1995).
10. C. Canuto, M. Y. Hassaini, A. Quarteroni, and T. A. Zang, *Spectral Methods in Fluid Dynamics*, 3rd ed. (Springer-Verlag, New York, 1988).
11. P. Codastefano, A. Di Russo, and V. Zanza, *Rev. Sci. Instrum.* **48**:1650 (1977).
12. H. S. Harned and R. L. Nuttall, *J. Am. Chem. Soc.* **69**:736 (1947).
13. L. B. Jalbert, R. M. Banish, and F. Rosenberger, *Phys. Rev. E.* **57**:1727 (1998).
14. L. B. Jalbert, F. Rosenberger, and R. M. Banish, *J. Phys.: Condens. Matter.* **10**:7113 (1998).
15. R. M. Banish, J. I. D. Alexander, and L. B. Jalbert, *Rev. Sci. Instrum.* **71**:4497 (2000).
16. A. G. Emslie and R. M. Banish, *Appl. Radiation and Isotopes* **54**:35 (2001).
17. T. Ida and R. I. L. Guthrie, *The Physical Properties of Liquid Metals* (Clarendon, Oxford, 1988).